Layer undulations in finite samples of smectic-*A* liquid crystals subjected to uniform pressure and magnetic fields

I. W. Stewart
Department of Mathematics, University of Strathclyde, Livingstone Tower, 26 Richmond Street, Glasgow G1 1XH, United Kingdom
(Received 12 June 1998)

This paper derives theoretical results for finite samples of smectic-*A* liquid crystals subjected to both a uniform pressure perpendicular to the smectic layers and a magnetic field applied in the plane of the layers or perpendicular to them; the special case of a uniform pressure with no field present is also considered. Criteria for suitable boundary conditions are derived for general finite sample geometries. Various critical field strengths are discussed in relation to the resulting gridlike smectic layer undulations which arise as solutions to the governing equation. A comparison is drawn with known results for infinite samples.
[S1063-651X(98)07211-0]

PACS number(s): 61.30.Cz, 87.22.−q

I. INTRODUCTION

The objective of this paper is to extend the work of Helfrich [1] and Hurault [2] for infinite samples of cholesteric liquid crystals under the influence of magnetic fields to finite samples of smectic-*A* liquid crystals subjected to both a uniform pressure and a magnetic field. Theoretical results for the Helfrich-Hurault transition in infinite samples of smectic-*A* liquid crystals under a magnetic field are well known, and can be found in de Gennes and Prost [3] and Chandrasekhar [4]. Smectic-*A* liquid crystals are layered anisotropic fluids. Each layer consists of long molecules whose average molecular alignment is perpendicular to the layers. The average alignment is denoted by the unit vector **n**, called the director. A typical sample alignment is indicated in Fig. 1, where we consider a smectic-*A* liquid crystal in a homeotropic alignment between two plates at a distance d apart in the z direction, and of finite dimensions a and b in the x and y directions, respectively. The coordinates adopted are as shown in Fig. 1, where the sample is confined to the volume Ω with $0\leqslant z\leqslant d$, $-a/2\leqslant x\leqslant a/2$ and $0\leqslant y\leqslant b$, chosen for convenience in discussing the solutions which arise below. It is further supposed that a small uniform constant pressure P is applied in the negative-z direction as shown, and that a magnetic field **H** may also be present in the x or z direction. The displacement of the layers is represented in the usual notation by $u(x,y,z)$. The corresponding smectic-*A* bulk elastic energy is (ignoring constant contributions) (Ref. [3], p. 343)

$$w_A=\frac{\overline{B}}{2}u_z^2+\frac{K_1}{2}[(u_{xx}+u_{yy})^2+4(u_{xy}^2-u_{xx}u_{yy})], \tag{1.1}$$

where $\overline{B}$ is the smectic layer compression constant and K_1 is the usual elastic splay constant. Throughout, suffices denote partial differentiation with respect to the variables indicated. For later convenience, the parameter λ is introduced as

$$\lambda=\sqrt{\left(\frac{K_1}{\overline{B}}\right)}, \tag{1.2}$$

which is a characteristic length of the material, of the order of the smectic layer thickness. Following Ref. [3], it is assumed that for small displacements to the initial alignment $\mathbf{n}_0$ the director **n** will be given by

$$\mathbf{n}\approx(-u_x,-u_y,1), \quad |u_x|,|u_y|\ll 1. \tag{1.3}$$

The relevant magnetic energies when a magnetic field **H** is applied parallel to the x axis or parallel to the z axis are, respectively (Ref. [3], pp. 119 and 344),

$$w_{Mx}=-\tfrac{1}{2}\chi_a(\mathbf{n}\cdot\mathbf{H})^2=-\tfrac{1}{2}\chi_a H^2u_x^2, \tag{1.4}$$

$$w_{Mz}=\tfrac{1}{2}\chi_a H^2(u_x^2+u_y^2), \tag{1.5}$$

where the constant terms have been omitted and $H=|\mathbf{H}|$. Notice that there is no minus sign in Eq. (1.5). For Eq. (1.4), it is supposed that the diamagnetic anisotropy χ_a is positive, which indicates that the director **n** ''prefers'' to align with the magnetic field when it is applied in the x direction: this will lead to a compression of the smectic layers. In Eq. (1.5) it is assumed that $\chi_a<0$, in which case the director will be repelled by a field in the z direction and the layers will compress. We consider separately the cases when **H** is parallel to the x and z axes in Secs. II and III below; it turns out that a solution involving Eq. (1.5) is easier to find since the governing equation is symmetric in x and y. The general bulk

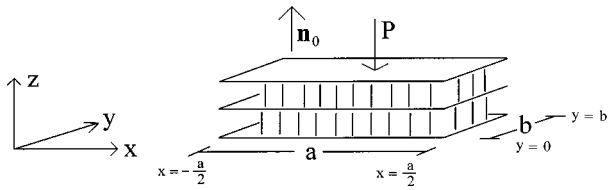

FIG. 1. The initial alignment of a planar sample of smectic-*A* liquid crystal. The average molecular alignment is parallel to the z axis and the similarly aligned molecules inherent in the smectic-*A* phase form equidistant layers as shown. A uniform constant pressure P is applied across the sample in the negative-z direction, and a magnetic field is present in the x or z direction. The sample is confined to the volume Ω where $0\leqslant z\leqslant d$, $-a/2\leqslant x\leqslant a/2$, and $0\leqslant y\leqslant b$.

equilibrium equations are given in Eqs. (2.14) and (3.1) below, while boundary conditions for general planar domains exhibiting a hinge flexibility (discussed below) are given in Eq. (2.12).

II. H PARALLEL TO *x* AXIS

The total energy integral is

$$W=\int_\Omega (w_A+w_{Mx})d\Omega=\int_\Omega\left[\frac{\overline{B}}{2}\,u_z^2+\frac{K_1}{2}\,(u_{xx}+u_{yy})^2+2K_1(u_{xy}^2-u_{xx}u_{yy})-\frac{1}{2}\,\chi_a H^2u_x^2\right]d\Omega. \tag{2.1}$$

To make the problem more tractable, we assume that the layer displacements are of small amplitude, and that we can make an approximation for u of the form

$$u=u_0\sin\left(\frac{\pi}{d}\,z\right)v(x,y), \tag{2.2}$$

with u_0 a small constant, allowing u to be zero on the boundaries $z=0$ and d. Inserting Eq. (2.2) into Eq. (2.1) gives

$$W=\frac{1}{2}\,du_0^2\int_S\left[\frac{\overline{B}}{2}\left(\frac{\pi}{d}\right)^2v^2+\frac{K_1}{2}\,(\Delta v)^2+2K_1(v_{xy}^2-v_{xx}v_{yy})-\frac{1}{2}\,\chi_a H^2v_x^2\right]dS \tag{2.3}$$

where S is the region $-a/2\leqslant x\leqslant a/2$, $0\leqslant y\leqslant b$, with boundary Γ, and Δ is the usual two-dimensional Laplace operator.

The work done by the constant pressure P per unit area in the xy plane on a thin layer of smectic-A liquid crystal is, using Eq. (2.2),

$$W_P=-\int_\Omega Pu\;d\Omega=-2u_0\,\frac{d}{\pi}\int_S Pv\;dx\;dy. \tag{2.4}$$

We now vary the integral

$$I=W+W_P, \tag{2.5}$$

where the variations $\eta(x,y)$ satisfy $\eta=0$ on Γ. We first note that integration by parts gives

$$\delta\int_S v_x^2dS=-2\int_S v_{xx}\eta dS \tag{2.6}$$

since $\eta=0$ for $x=\pm a/2$, and, therefore, applying the standard variation process, we obtain

$$\delta I=\frac{1}{2}\,u_0^2d\int_S\left[\overline{B}\left(\frac{\pi}{d}\right)^2v-\frac{4P}{\pi u_0}+\chi_aH^2v_{xx}\right]\eta\;dS+\frac{1}{2}\,u_0^2dK_1\delta\int_S\left[\frac{1}{2}\,(\Delta v)^2+2(v_{xy}^2-v_{xx}v_{yy})\right]dS. \tag{2.7}$$

The variation of the second integral in Eq. (2.7) has been discussed in great detail by Landau and Lifshitz (Ref. [5], Chap. 2). Let $\boldsymbol{\nu}$ and $\mathbf{1}$ denote the unit outward normal to Γ and the unit tangent vector to Γ, respectively, and suppose that the smectic layers are simply supported [5], in the sense that η must be zero on Γ while $\partial\eta/\partial\nu$ may be arbitrary. This means that the layers are allowed to possess a ''hinge'' flexibility with no displacement on Γ. For variations which vanish on Γ it can be shown that (Ref. [5], p. 42, with $\sigma=-1$)

$$\delta\int_S\left[\frac{1}{2}\,(\Delta v)^2+2(v_{xy}^2-v_{xx}v_{yy})\right]dS=\int_S(\Delta^2v)\,\eta dS+\oint_\Gamma[\Delta v+2(2\sin\theta\,\cos\theta v_{xy}-\sin^2\theta v_{xx}-\cos^2\theta v_{yy})]\,\frac{\partial\eta}{\partial\nu}\,dl-\oint_\Gamma\left[\frac{\partial\Delta v}{\partial n}+2\,\frac{\partial}{\partial l}\,\{\sin\theta\,\cos\theta(v_{yy}-v_{xx})+(\cos^2\theta-\sin^2\theta)v_{xy}\}\right]\eta dl, \tag{2.8}$$

where θ is the angle between the x axis and the outward normal $\boldsymbol{\nu}$ to Γ, and Δ^2 is the biharmonic operator

$$\Delta^2=\frac{\partial^4}{\partial x^4}+2\,\frac{\partial^4}{\partial x^2\partial y^2}+\frac{\partial^4}{\partial y^4}. \tag{2.9}$$

From Eqs. (2.7) and (2.8), it is seen that, at equilibrium, that is when $\delta I=0$, we require, in S,

$$\int_S\left[\overline{B}\left(\frac{\pi}{d}\right)^2v-\frac{4P}{\pi u_0}+\chi_aH^2v_{xx}+K_1\Delta^2v\right]\eta dS=0 \tag{2.10}$$

and, since $\eta=0$ and $\partial\eta/\partial\nu$ is arbitrary on Γ,

$$\oint_\Gamma[\Delta v+2(2\sin\theta\,\cos\theta v_{xy}-\sin^2\theta v_{xx}-\cos^2\theta v_{yy})]\,\frac{\partial\eta}{\partial\nu}\,dl=0. \tag{2.11}$$

Equations (2.10) and (2.11) are the governing equilibrium equations on S and Γ, respectively. For the aforementioned simply supported boundary conditions the terms between the square brackets in Eq. (2.11) equate to zero on Γ when (Ref. [5], p. 44)

$$v=0\quad\text{and}\quad\frac{\partial^2v}{\partial\nu^2}-\frac{d\theta}{dl}\,\frac{\partial v}{\partial\nu}=0. \tag{2.12}$$

Equations (2.12) are quite general for simply supported conditions, and will be applicable for any shape of domain in the xy plane. In the geometry of Fig. 1, θ is always a constant, and therefore the boundary conditions which are required are

$$v=0 \quad \text{on } \Gamma,$$

$$v_{xx}=0 \quad \text{for } x=\pm\frac{a}{2},$$

$$v_{yy}=0 \quad \text{for } y=0 \text{ and } b. \tag{2.13}$$

With the above boundary conditions, Eq. (2.11) is automatically satisfied, and therefore our attention is focused upon the bulk equilibrium equation which arises from Eq. (2.10). From the arbitrariness of η in S, this can be written, using Eq. (1.2), as

$$\Delta^2 v+\frac{\chi_a}{K_1}H^2 v_{xx}=\frac{4P}{\pi K_1 u_0}-\left(\frac{\pi}{d\lambda}\right)^2 v. \tag{2.14}$$

The problem is now reduced to solving Eq. (2.14) with the boundary conditions (2.13).

We now adapt the solution given by Timoshenko (Ref. [6], p. 270) to suit the above boundary conditions and additional magnetic field terms, anticipating that the solution will not be symmetrical in x and y when $H>0$. (A symmetrical Navier-type double series solution in x and y for $H=0$ is discussed in Sec. III below.) The basic method is to find a particular solution $v_1(y)$ of Eq. (2.14), and add to it a general solution $v_2(x,y)$ of the homogeneous version of Eq. (2.14); the full solution is then given by $v(x,y)=v_1(y)+v_2(x,y)$. First, note that the half-range Fourier sine series of the constant term in Eq. (2.14) is given by

$$\frac{4P}{K_1\pi u_0}=\frac{16P}{K_1\pi^2 u_0}\sum_{n=1,3,5,\ldots}^{\infty}\frac{1}{n}\sin\left(\frac{n\pi y}{b}\right), \quad 0<y<b. \tag{2.15}$$

The series $v_1(y)$ defined by

$$v_1(y)=\sum_{n=1,3,5,\ldots}^{\infty}P_n\sin\left(\frac{n\pi y}{b}\right) \tag{2.16}$$

furnishes a particular solution to Eq. (2.14) provided the coefficients P_n are

$$P_n=\frac{16P}{K_1\pi^2 u_0}\frac{1}{n}\left[\left(\frac{n\pi}{b}\right)^4+\left(\frac{\pi}{d\lambda}\right)^2\right]^{-1}. \tag{2.17}$$

Hence $v_1(y)$ given by Eqs. (2.16) and (2.17) is a particular solution to Eq. (2.14). We now seek a solution $v_2(x,y)$ of the form

$$v_2(x,y)=\sum_{n=1,3,5,\ldots}^{\infty}Y_n(x)\sin\left(\frac{n\pi y}{b}\right) \tag{2.18}$$

to the homogeneous equation

$$\Delta^2 v+\frac{\chi_a}{K_1}H^2 v_{xx}+\left(\frac{\pi}{d\lambda}\right)^2 v=0. \tag{2.19}$$

Inserting Eq. (2.18) into Eq. (2.19) yields the differential equation for the Y_n coefficients

$$Y_n^{(4)}(x)+\left[\frac{\chi_a}{K_1}H^2-2\left(\frac{n\pi}{b}\right)^2\right]Y_n^{(2)}(x)+\left[\left(\frac{n\pi}{b}\right)^4+\left(\frac{\pi}{d\lambda}\right)^2\right]Y_n(x)=0. \tag{2.20}$$

The eigenvalues for Eq. (2.20) are

$$\beta_n\pm\gamma_n i, \quad -\beta_n\pm\gamma_n i, \tag{2.21}$$

where

$$\beta_n^2=\frac{1}{2}\left\{\left[\left(\frac{n\pi}{b}\right)^4+\left(\frac{\pi}{d\lambda}\right)^2\right]^{1/2}+\left(\frac{n\pi}{b}\right)^2-\frac{\chi_a H^2}{2K_1}\right\}, \tag{2.22}$$

$$\gamma_n^2=\frac{1}{2}\left\{\left[\left(\frac{n\pi}{b}\right)^4+\left(\frac{\pi}{d\lambda}\right)^2\right]^{1/2}-\left(\frac{n\pi}{b}\right)^2+\frac{\chi_a H^2}{2K_1}\right\}. \tag{2.23}$$

Notice that γ_n^2 is always positive, since it is assumed here that $\chi_a>0$. These eigenvalues lead to the consideration of three main types of solution, namely, when β_n^2 is positive, zero, or negative.

A. $\beta_n^2>0$

The β_n^2 terms are positive only when

$$\frac{\chi_a}{2K_1}H^2<\left[\left(\frac{n\pi}{b}\right)^4+\left(\frac{\pi}{d\lambda}\right)^2\right]^{1/2}+\left(\frac{n\pi}{b}\right)^2. \tag{2.24}$$

For convenience, define

$$H_n=\left(2\frac{K_1}{\chi_a}\left\{\left[\left(\frac{n\pi}{b}\right)^4+\left(\frac{\pi}{d\lambda}\right)^2\right]^{1/2}+\left(\frac{n\pi}{b}\right)^2\right\}\right)^{1/2}. \tag{2.25}$$

Then

$$\beta_n^2>0$$

for all n only when

$$H<H_1. \tag{2.26}$$

We remark that as $b\to\infty$ in Eq. (2.25) the critical field strength for an infinite sample (see Ref. [3], p. 363) is recovered, namely,

$$H_c=\left(2\frac{K_1}{\chi_a}\frac{\pi}{d\lambda}\right)^{1/2}. \tag{2.27}$$

The four forms of solution for $Y_n(x)$ are

$$\cosh\beta_n x\cos\gamma_n x, \quad \sinh\beta_n x\sin\gamma_n x, \tag{2.28}$$

$$\cosh\beta_n x\sin\gamma_n x, \quad \sinh\beta_n x\cos\gamma_n x. \tag{2.29}$$

Since the full solution sought is even in x, the solutions for Y_n in Eq. (2.29) can be disregarded. Hence the general solution to Eq. (2.20) is

$$Y_n(x)=A_n\cosh\ \beta_n x\ \cos\ \gamma_n x+B_n\sinh\ \beta_n x\ \sin\ \gamma_n x. \tag{2.30}$$

From Eqs. (2.16), (2.18), and (2.30) the general solution to Eq. (2.14) is then the single series

$$\begin{aligned} v(x,y)&=v_1(y)+v_2(x,y)\\ &=\sum_{n=1,3,5,\ldots}^{\infty}[P_n+A_n\cosh\ \beta_n x\ \cos\ \gamma_n x\\ &\quad+B_n\sinh\ \beta_n x\ \sin\ \gamma_n x]\sin\left(\frac{n\pi y}{b}\right), \end{aligned} \tag{2.31}$$

where the coefficients A_n and B_n are to be determined from the boundary conditions (2.13). A double series Navier solution, using the form of the series in Eq. (3.4) below, can be shown to be equivalent to the above single series solution: shift the domain of x to $0\leqslant x\leqslant a$ and rewrite $Y_n(x)$ in Eq. (2.30) as a Fourier sine series in x on this interval. In this present case the details of eigenvalues and how critical parameters change are of relevance, and this information is explicitly available with the single series method.

Insertion of $v(x,y)$ and its second derivatives into Eq. (2.14) shows that in order to fulfill the boundary conditions (2.13) the constant coefficients A_n and B_n have to satisfy the equations

$$\begin{bmatrix} c_n^{11} & c_n^{12}\\ c_n^{21} & c_n^{22}\end{bmatrix}\begin{bmatrix} A_n\\ B_n\end{bmatrix}=\begin{bmatrix} -P_n\\ 0\end{bmatrix}, \tag{2.32}$$

where the entries in the above matrix $C_n=(c_n^{ij})$ are

$$c_n^{11}=\cosh\left(\frac{\beta_n a}{2}\right)\cos\left(\frac{\gamma_n a}{2}\right), \tag{2.33}$$

$$c_n^{12}=\sinh\left(\frac{\beta_n a}{2}\right)\sin\left(\frac{\gamma_n a}{2}\right), \tag{2.34}$$

$$\begin{aligned} c_n^{21}&=(\beta_n^2-\gamma_n^2)\cosh\left(\frac{\beta_n a}{2}\right)\cos\left(\frac{\gamma_n a}{2}\right)\\ &\quad-2\beta_n\gamma_n\ \sinh\left(\frac{\beta_n a}{2}\right)\sin\left(\frac{\gamma_n a}{2}\right), \end{aligned} \tag{2.35}$$

$$\begin{aligned} c_n^{22}&=(\beta_n^2-\gamma_n^2)\sinh\left(\frac{\beta_n a}{2}\right)\sin\left(\frac{\gamma_n a}{2}\right)\\ &\quad+2\beta_n\gamma_n\cosh\left(\frac{\beta_n a}{2}\right)\cos\left(\frac{\gamma_n a}{2}\right). \end{aligned} \tag{2.36}$$

The determinant of C_n is

$$\begin{aligned} \det(C_n)&=2\beta_n\gamma_n\left[\cosh^2\left(\frac{\beta_n a}{2}\right)\cos^2\left(\frac{\gamma_n a}{2}\right)\right.\\ &\quad\left.+\sinh^2\left(\frac{\beta_n a}{2}\right)\sin^2\left(\frac{\gamma_n a}{2}\right)\right]. \end{aligned} \tag{2.37}$$

By Eq. (2.26), $\beta_n^2>0$ for all n only when $H<H_1$, while γ_n^2 is always positive. Therefore,

$$\det(C_n)\neq 0$$

for all n whenever

$$0<H<H_1. \tag{2.38}$$

Hence for $0<H<H_1$, system (2.32) has the unique solutions

$$A_n=\frac{-P_n c_n^{22}}{\det(C_n)}, \tag{2.39}$$

$$B_n=\frac{P_n c_n^{21}}{\det(C_n)}, \tag{2.40}$$

for each $n=1,3,5,\ldots$. The final full solution to Eqs. (2.13) and (2.14) is now given by Eq. (2.31), with Eqs. (2.17), (2.37), (2.39), and (2.40).

In order to gain insight into the behavior of solution (2.31), the first term in the series may be taken as an approximation to $v(x,y)$: therefore we look at

$$\begin{aligned} V(x,y)&=[P_1+A_1\cosh\ \beta_1 x\ \cos\ \gamma_1 x\\ &\quad+B_1\sinh\ \beta_1 x\ \sin\ \gamma_1 x]\sin\left(\frac{\pi y}{b}\right). \end{aligned} \tag{2.41}$$

Since P is arbitrary in Eq. (2.17) and occurs in P_1, A_1, and B_1, we can suppose for the present discussion (since u_0 is arbitrary) that $P_1=1$, and use Eqs. (2.33)–(2.40) to calculate V in Eq. (2.41) numerically, and display the corresponding results. For simplicity, and clarity of exposition, we choose the following (in cgs units):

$$b=\pi,\quad a=\pi,\quad d\lambda=\pi\times 10^{-2},\quad K_1=10^{-6},\quad \chi_a=10^{-7}. \tag{2.42}$$

These values for K_1 and χ_a are the same as those used in Ref. [3], p. 363, where $d\lambda=2\times 10^{-10}$; the choice for $d\lambda$ in Eq. (2.42) will not affect the qualitative aspects of the graphs shown below, since the effect of decreasing $d\lambda$ is to increase β_1, γ_1, and H_1. The case for $d\lambda=2\times 10^{-10}$ is commented upon at the end of this section.

For the values in Eq. (2.42),

$$H_1=44.95. \tag{2.43}$$

For H approaching H_1 from below, consider $H=40$ and the corresponding values

$$\begin{aligned} &\beta_1=3.24,\quad \gamma_1=9.46,\quad A_1=2.00\times 10^{-2},\\ &B_1=1.27\times 10^{-3}. \end{aligned} \tag{2.44}$$

We can assume u_0 is arbitrary, and examine the displacement in the $z=d/2$ midplane in order to gain insight into the full solution. The resulting approximate displacement $V(x,y)$ is given as a surface plot in Fig. 2(a), with the corresponding contour plot drawn in the lower xy plane. The greatest displacement occurs at $y=\pi/2$ where, as can be seen in the figure, the oscillatory behavior of the solution becomes

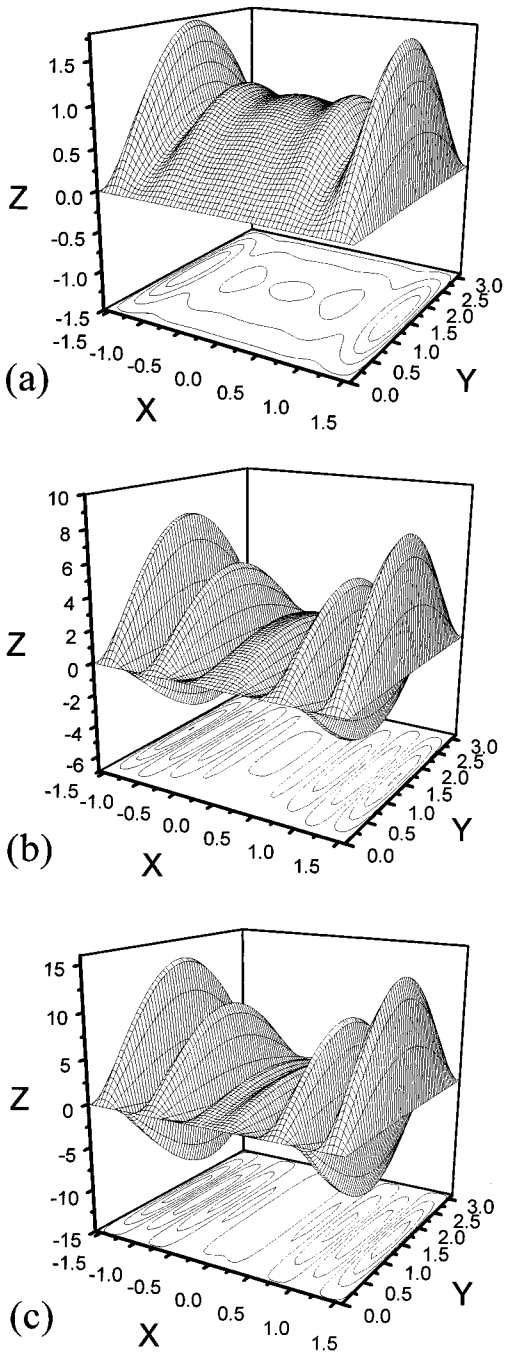

FIG. 2. Surface and contour plots for the approximating solution $V(x,y)$, given by Eq. (2.41), to the layer displacement u for the parameters in Eq. (2.42) with $P_1=1$. The magnetic field $\boldsymbol{H}$ is parallel to the x axis. (a) $H=40$, (b) $H=H_1=44.95$, and (c) $H=45.166$. In all three plots the largest amplitude of the undulations occurs near the boundaries at $x=\pm\pi/2$.

most apparent. The number of ''peaks'' and ''troughs'' is approximately γ_1. This is to be expected since for a given value of H the period of the oscillatory terms is $2\pi/\gamma_1$ and, because $-\pi/2\leqslant x\leqslant\pi/2$, the number of oscillations is approximately $\gamma_1/2$. The largest amplitude of the undulations occurs near the boundaries at $x=\pm a/2=\pm\pi/2$.

B. $\beta_1^2=0$, $\beta_n^2>0$, $n\geqslant 2$

Clearly, $\det(C_n)$ is first zero when $n=1$ and $\beta_1=0$ at $H=H_1$. For $n\geqslant 2$ the solutions remain in the same form as in Eqs. (2.32)–(2.40). At $H=H_1$ there are two repeated eigenvalues $\pm\gamma_1 i$, and hence the solutions which are even in x are

$$\cos\gamma_1 x, \quad x\,\sin\gamma_1 x. \tag{2.45}$$

Therefore the corresponding solution to Eq. (2.41) is

$$V(x,y)=[P_1+A_1\cos\gamma_1 x+B_1 x\,\sin\gamma_1 x]\sin\left(\frac{\pi y}{b}\right). \tag{2.46}$$

As in Eq. (2.32), the matrix of coefficients C_1 is formed whose entries in this case are

$$c_1^{11}=\cos\left(\frac{\gamma_1 a}{2}\right), \tag{2.47}$$

$$c_1^{12}=\frac{a}{2}\,\sin\left(\frac{\gamma_1 a}{2}\right), \tag{2.48}$$

$$c_1^{21}=-\gamma_1^2\cos\left(\frac{\gamma_1 a}{2}\right), \tag{2.49}$$

$$c_1^{22}=2\gamma_1\cos\left(\frac{\gamma_1 a}{2}\right)-\frac{a\gamma_1^2}{2}\,\sin\left(\frac{\gamma_1 a}{2}\right), \tag{2.50}$$

with the determinant

$$\det(C_1)=2\gamma_1\cos^2\left(\frac{\gamma_1 a}{2}\right). \tag{2.51}$$

With these values, A_1 and B_1 are given by Eqs. (2.39) and (2.40). Also, the solution given by Eqs. (2.46)–(2.50) can be obtained by carefully taking the limit as $\beta\to 0$ in Eq. (2.41) using Eqs. (2.33)–(2.40). At $H=H_1$ we have

$$\beta_1=0, \quad \gamma_1=10.00, \quad A_1=0.997, \quad B_1=5.00. \tag{2.52}$$

There is the possibility that $\det(C_1)=0$ for certain values of H. However, for the parameters discussed here, $\det(C_1)\neq 0$. Again, $P_1=1$ is chosen for convenience, and the resulting plots for Eq. (2.46) are shown in Fig. 2(b). As before, the largest amplitude of the undulations occurs near the boundaries at $x=\pm\pi/2$.

C. $\beta_1^2<0$, $\beta_n^2>0$, $n\geqslant 2$

For $H>H_1$ the eigenvalues at $n=1$ for Eq. (2.20) are

$$(|\beta_1|\pm\gamma_1)i, \quad (-|\beta_1|\pm\gamma_1)i, \tag{2.53}$$

the other eigenvalues remaining the same as in Eq. (2.21) provided

$$H<H_3=46.777. \tag{2.54}$$

Using an identical approach to that in Sec. II A above, this leads to a solution of the form in Eq. (2.31) except that the term for $n=1$ in the series is replaced by

$$V(x,y)=[P_1+A_1\cos(|\beta_1|x)\cos\ \gamma_1 x + B_1\sin(|\beta_1|x)\sin\ \gamma_1 x]\sin\left(\frac{\pi y}{b}\right). \quad (2.55)$$

As before, the matrix C_1 is calculated from the boundary conditions and found to have the entries

$$c_1^{11}=\cos\left(\frac{|\beta_1|a}{2}\right)\cos\left(\frac{\gamma_1 a}{2}\right), \quad (2.56)$$

$$c_1^{12}=\sin\left(\frac{|\beta_1|a}{2}\right)\sin\left(\frac{\gamma_1 a}{2}\right), \quad (2.57)$$

$$c_1^{21}=2|\beta_1|\gamma_1\sin\left(\frac{|\beta_1|a}{2}\right)\sin\left(\frac{\gamma_1 a}{2}\right) - (|\beta_1|^2+\gamma_1^2)\cos\left(\frac{|\beta_1|a}{2}\right)\cos\left(\frac{\gamma_1 a}{2}\right), \quad (2.58)$$

$$c_1^{22}=2|\beta_1|\gamma_1\cos\left(\frac{|\beta_1|a}{2}\right)\cos\left(\frac{\gamma_1 a}{2}\right) - (|\beta_1|^2+\gamma_1^2)\sin\left(\frac{|\beta_1|a}{2}\right)\sin\left(\frac{\gamma_1 a}{2}\right), \quad (2.59)$$

with

$$\det(C_1)=2|\beta_1|\gamma_1\left[\cos^2\left(\frac{|\beta_1|a}{2}\right)\cos^2\left(\frac{\gamma_1 a}{2}\right) - \sin^2\left(\frac{|\beta_1|a}{2}\right)\sin^2\left(\frac{\gamma_1 a}{2}\right)\right]. \quad (2.60)$$

The values for A_1 and B_1 are now given by these results and Eqs. (2.39) and (2.40). We first observe that

$$\det(C_1)=0$$

whenever

$$|\beta_1|+\gamma_1=(2k-1)\frac{\pi}{a}, \quad k=1,2,3,\ldots . \quad (2.61)$$

When Eqs. (2.61) hold, system (2.32) remains consistent at $n=1$, but includes an indeterminacy since one of the constants A_1 or B_1 can be chosen arbitrarily. Also, both the coefficients A_1 and B_1 diverge as H approaches the first zero for $\det(C_1)$ above H_1. For the same values discussed above in Eq. (2.42),

$$\det(C_1)=0 \quad \text{when} \quad H=45.349, \quad (2.62)$$

and for an example we therefore consider $H=45.166$, which is above H_1 but below the first value for which the $\det(C_1)=0$; also, $H<H_3$ given by Eq. (2.54) in this case. For this value of H we have

$$|\beta_1|=0.705, \quad \gamma_1=10.025,$$
$$A_1=0.982, \quad B_1=15.930. \quad (2.63)$$

For these values, with $P_1=1$, the approximating solution is plotted in Fig. 2(c) where again the largest amplitude of the undulations occurs near the boundaries at $x=\pm\pi/2$. For $\beta_n=0$ and $n\geqslant 2$, the procedure above for $n=1$ can be repeated for each term in the series solution (2.31), but the details are omitted since the dominating behavior for the full series solution is expected to be the first term at $n=1$.

It is worth remarking that the form of the solution changes smoothly as H increases through H_1, because the form in Eq. (2.46) can be obtained as a limit as $H\to H_1$ from above or below. The solution only breaks down when H reaches the value for which $\det(C_1)$ first equals zero, as in Eq. (2.62): as H approaches such a value the amplitude of the oscillatory terms tends to infinity. The solutions in Fig. 2 display what is essentially a one-dimensional pattern along the x-direction.

In all of the examples above, $d\lambda=\pi\times 10^{-2}$. For a more physically relevant value we can take $d\lambda=2\times 10^{-10}$ to find that, with the other values remaining the same as in Eq. (2.42), $H_1\approx 560\,499=56.04\,99$ kG. In this case, for H close to H_1, for example $H=560\,400$, $\gamma_1\approx 1.25\times 10^5$, indicating that there are many more oscillations than those appearing in the figures presented above, but that the qualitative aspects remain identical. Further, the critical field (2.27) discussed in Ref. [3] for an infinite sample is approximately that given by H_1 in this case.

III. *H* PARALLEL TO THE *z* AXIS

When H is parallel to the z axis, the analysis of Sec. II can be repeated up to Eq. (2.14) with the magnetic field term being replaced by that resulting from w_{Mz} in Eq. (1.5). The equation to be solved is therefore

$$\Delta^2 v-\frac{\chi_a}{K_1}H^2(v_{xx}+v_{yy})=\frac{4P}{\pi K_1 u_0}-\left(\frac{\pi}{d\lambda}\right)^2 v \quad (3.1)$$

with $\chi_a<0$. The equation is symmetric in x and y, and the solution is expected to reflect this property. For simplicity therefore we shift the x coordinate by $a/2$ so that the boundary conditions (2.13) become

$$v=0 \quad \text{on} \quad \Gamma,$$
$$v_{xx}=0 \quad \text{for} \quad x=0,a,$$
$$v_{yy}=0 \quad \text{for} \quad y=0,b. \quad (3.2)$$

A Navier-type solution will now be sought (Ref. [6], p. 272). We begin by writing the constant term in (3.1) as the double half-range Fourier series

$$\frac{4P}{K_1\pi u_0}=\frac{64P}{K_1\pi^3 u_0}\sum_{n=1,3,5,\ldots}^{\infty}\sum_{m=1,3,5,\ldots}^{\infty}\frac{1}{mn}\sin\left(\frac{m\pi x}{a}\right)\times\sin\left(\frac{n\pi y}{b}\right), \quad 0<x<a, \quad 0<y<b. \quad (3.3)$$

The series

$$v(x,y)=\sum_{n=1,3,5,\ldots}^{\infty}\sum_{m=1,3,5,\ldots}^{\infty}A_{mn}\sin\left(\frac{m\pi x}{a}\right)\sin\left(\frac{n\pi y}{b}\right), \tag{3.4}$$

when inserted with Eq. (3.3) into Eq. (3.1), is a solution satisfying the boundary conditions (3.2), provided

$$A_{mn}=\frac{64P}{K_1\pi^3u_0}\frac{1}{mn}\left\{\left[\left(\frac{m\pi}{a}\right)^2+\left(\frac{n\pi}{b}\right)^2\right]^2+\left(\frac{\pi}{d\lambda}\right)^2+\frac{\chi_a}{K_1}H^2\left[\left(\frac{m\pi}{a}\right)^2+\left(\frac{n\pi}{b}\right)^2\right]\right\}^{-1}. \tag{3.5}$$

The coefficient of A_{mn} becomes singular as a function of H when H satisfies

$$-\frac{\chi_a}{K_1}H^2=\left(\frac{m\pi}{a}\right)^2+\left(\frac{n\pi}{b}\right)^2+\left(\frac{\pi}{d\lambda}\right)^2\left[\left(\frac{m\pi}{a}\right)^2+\left(\frac{n\pi}{b}\right)^2\right]^{-1}. \tag{3.6}$$

The minimum value of the right-hand side of Eq. (3.6) with respect to m and n occurs when

$$\left(\frac{m\pi}{a}\right)^2+\left(\frac{n\pi}{b}\right)^2=\frac{\pi}{d\lambda}. \tag{3.7}$$

In general, Eq. (3.7) will not be satisfied by any integers m and n, but the terms in the series which will have maximum amplitude can be determined from the values of m and n which give the closest approximation to Eq. (3.7). Also, when Eq. (3.7) holds, the critical value of H is found, from Eq. (3.6), to be

$$H_c=\left(-2\frac{K_1}{\chi_a}\frac{\pi}{d\lambda}\right)^{1/2}, \tag{3.8}$$

which is the critical-field result analogous to Eq. (2.27) for an infinite sample.

As an example we take the values in Eq. (2.42), except that $\chi_a=-10^{-7}$, to find that the (odd) values of m and n which give the closest approximation to $\pi/d\lambda=100$ are

$$m=n=7, \tag{3.9}$$

indicating that the term involving A_{77} contains the dominant modes as H approaches Eq. (3.8) from below. Since Eq. (3.7) is not identically satisfied for these particular values, the solution is actually valid until H finally satisfies Eq. (3.6) for $m=n=7$, which is slightly above the value given by Eq. (3.8). Here $H_c=44.7214$, while the solution actually becomes singular at $H=44.7259$. As in Sec. II, we examine the solution around the midplane $z=d/2$. The sum of the first ten terms in the solution series (3.4) with Eq. (3.5) are plotted as surfaces and contour plots for

$$u_0=\frac{64P}{K_1\pi^3} \tag{3.10}$$

for three values of H. Figure 3(a) shows this solution for $H=0$, and Fig. 3(b) is the solution for $H=42.2719$, which is below H_c. Figure 3(c) is the solution for $H=H_c=44.7214$. In all of these plots the largest amplitude of the undulations occurs near the four corners in the xy plane. At $H=H_c$ there is an approximate two-dimensional gridlike pattern reminiscent of the square-grid pattern (see Ref. [4], p. 282, for experimental observations by Rondelez) induced by a magnetic field in cholesteric liquid crystals, first proposed theoretically

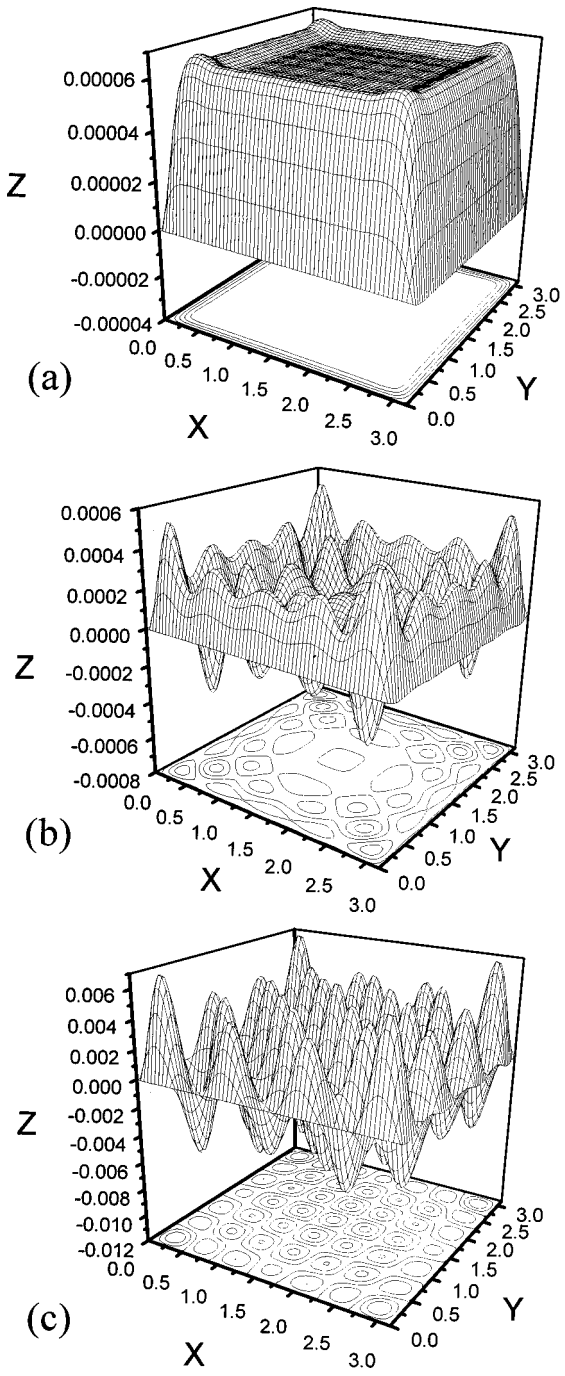

FIG. 3. Surface and contour plots for the sum of the first ten terms in the series solution (3.4) representing the layer displacement u at the midplane $z=d/2$ for u_0 given by Eq. (3.10). The parameters are as in Eq. (2.42), except that $\chi_a=-10^{-7}$. The magnetic field is parallel to the z direction with $0\leq x\leq a$ and $0\leq y\leq b$. (a) $H=0$, (b) $H=42.2719$, and (c) $H=H_c=44.7214$. In all of these plots the largest amplitude of the undulations occurs near the four corners in the xy plane. In (c), for these parameters, there is a 7×7 contour grid, corresponding to the dominant mode containing A_{77} in Eq. (3.4), as discussed in the text.

by Helfrich [1] and Hurault [2]. As commented upon in Sec. II a typical, more physically meaningful, value of $d\lambda = 2 \times 10^{-10}$ lends itself to a similar analysis, the only difference being the much greater number of grids appearing as H approaches H_c.

IV. DISCUSSION

Figures 2 and 3 graphically summarize the results for the layer displacement u of a homeotropically aligned sample of smectic-A liquid crystal confined to a finite geometry and subjected to a uniform constant pressure P and an applied magnetic field. Figure 2 represents an approximate solution to u in the $z = d/2$ midplane of the sample (for the geometry depicted in Fig. 1), where $\boldsymbol{H}$ is in the plane of the layers in the x direction, and $\chi_a > 0$. In Fig. 3, $\boldsymbol{H}$ is in the z direction (perpendicular to the layers), and $\chi_a < 0$. The effect of increasing the magnitude of the magnetic field has been shown in these graphs via the equations discussed in Secs. II and III. Figure 2 has contour patterns along the x direction, and Fig. 3 has grid contour patterns in the xy plane. The solutions were shown to change mathematical form as H reached certain critical values, depending on the physical parameters. These results share similar features to those presented by Fukuda and Onuki [7], who numerically examined the dynamics of layer undulation instabilities in samples of smectic-A liquid crystals (infinite in the x and y directions) induced by an external field; square-grid patterns occur as the dynamical system progresses to its final state when the field is perpendicular to the layers, while a one-dimensional pattern occurs when the field is parallel to the layers.

The assumption of simply supported boundary conditions, which lead to the boundary equations in Eq. (2.12), can perhaps be relaxed to incorporate variations which do not necessarily satisfy $\eta = 0$ on the boundary Γ; this introduces more intricate mathematics and other forms of variations are currently being investigated. The physical boundaries in smectic samples are well known to be much more complex than those presented here due to defects and focal conics. Nevertheless, at a small distance from the actual boundary the smectic liquid crystal may well behave as though it has a hinge flexibility near the boundary, so that, mathematically, the boundary conditions proposed in this paper have some physical significance.

Pressure, for example, applied over a small-xy region can be analyzed in an identical fashion to that presented here by introducing a suitable single or double half-range Fourier series for P to replace Eqs. (2.15) or (3.3). Analytical work is currently in progress by the author for various forms of P using the techniques employed by Timoshenko [6] for concentrated loads on rectangular plates. It should also be mentioned that layer undulations in smectic-A liquid crystals may be induced via a dilation of the layers imposed by mechanical tension [3,4]. Also, Ribotta and Durand [8] have experimentally observed smectic-A liquid crystals under dilation or compression, and found two possible forms of instability: undulation of the layers or molecular tilt within the layers.

A natural extension to the work presented here is to consider the smectic-C phase where the director $\mathbf{n}$ is tilted at an angle θ (the smectic cone angle) to the layer normal [3]. The onset of layer deformations in nonchiral smectic-C liquid crystals induced by an electric field in the absence of external pressure has been examined theoretically by Kedney and Stewart [9] using the smectic continuum theory of Leslie and co-workers [10,11]. In Ref. [9] the layer structure cannot be as easily visualized as in this present paper, due to the approximations used from the nonlinear theory in Refs. [10, 11], although an approximate critical threshold for the onset of layer undulations can be derived. A recent nonlinear theory which allows layer dilation and compression has been proposed by McKay and Leslie [12] in an attempt to gain more information on the static layer structure of compressible smectic-C liquid crystals in a homeotropic alignment. Such an alignment under an ac electric field has been studied experimentally by Ruan, Sambles, and Towler [13], who reported an increase in the smectic cone angle for smectic-C liquid crystals, but not a Helfrich-type effect. Layer relaxations of chevrons in smectic-C^* liquid crystals and layer undulations in the dilative mode, based upon a continuum theory of compressible smectics, has been investigated by Mukai and Nakagawa [14] for a ''bookshelf'' geometry. An analysis of the type presented here may well be of interest for the smectic problems examined in these references when external pressure terms are incorporated into the models.

ACKNOWLEDGMENTS

The author wishes to express his thanks to G. J. Barclay and J. E. Kidd for their valuable comments on this and related work on smectic undulations.

[1] W. Helfrich, J. Chem. Phys. **55**, 839 (1971).
[2] J. P. Hurault, J. Chem. Phys. **59**, 2068 (1973).
[3] P. G. de Gennes and J. Prost, *The Physics of Liquid Crystals* (Clarendon, Oxford, 1993).
[4] S. Chandrasekhar, *Liquid Crystals*, 2nd ed. (Cambridge University Press, Cambridge, 1992).
[5] L. D. Landau and E. M. Lifshitz, *Theory of Elasticity*, 3rd ed. (Pergamon, Oxford, 1986).
[6] S. Timoshenko and S. Woinowsky-Krieger, *Theory of Plates and Shells*, 2nd ed. (McGraw-Hill, New York, 1987).
[7] J. Fukuda and A. Onuki, J. Phys. II **5**, 1107 (1995).
[8] R. Ribotta and G. Durand, J. Phys. (Paris) **38**, 179 (1977).
[9] P. J. Kedney and I. W. Stewart, ZAMP **45**, 882 (1994).
[10] F. M. Leslie, I. W. Stewart, and M. Nakagawa, Mol. Cryst. Liq. Cryst. **198**, 443 (1991).
[11] F. M. Leslie, I. W. Stewart, T. Carlsson, and M. Nakagawa, Continuum. Mech. Thermodyn. **3**, 237 (1991).
[12] G. McKay and F. M. Leslie, Eur. J. Appl. Math. **8**, 273 (1997).
[13] L. Ruan, J. R. Sambles, and M. J. Towler, Liq. Cryst. **18**, 81 (1995).
[14] S. Mukai and M. Nakagawa, Jpn. J. Appl. Phys. **33**, 6255 (1994).